Carrier and field dynamics around nanoscale Schottky contacts investigated by ultrafast near-field optics

M. Achermann* and F. Morier-Genoud
Swiss Federal Institute of Technology Zurich, Institute of Quantum Electronics, ETH Honggerberg-HPT, CH-8093 Zurich, Switzerland

W. Seifert and L.-E. Wernersson
Solid State Physics/Nanometer Structure Consortium Lund University, Box 118, S-221 00 Lund, Sweden

U. Siegner
Physikalisch-Technische Bundesanstalt, D-38116 Braunschweig, Germany

U. Keller
Swiss Federal Institute of Technology Zurich, Institute of Quantum Electronics, ETH Honggerberg-HPT, 8093 Zurich, Switzerland
(Received 7 June 2001; published 7 January 2002)

We present femtosecond-resolved optical near-field pump-probe measurements of spatiotemporal carrier dynamics around a single nanoscale tungsten (W) disk embedded in GaAs. In these samples, Schottky contacts are formed at the W/GaAs interface. The experimental results are modeled by a selfconsistent treatment of the drift-diffusion equation for the carriers and Poisson's equation for the built-in electric field. At lower optically excited carrier densities, we observe that the built-in field suppresses electron transport towards and trapping into the metal particles. In this regime, an accumulation of carriers is seen at the edge of the depletion region of the Schottky contacts. The calculation reveals that the formation of a self-induced dynamic potential well is the origin of this result. In the high-density regime, efficient carrier transport towards and trapping into the W nanoparticle take place, resulting from the screening of the built-in field. These results allow us to describe measurements of the carrier dynamics in annealed low-temperature grown GaAs and demonstrate that the coupling of the carrier and field dynamics can substantially affect carrier trapping in metal-semiconductor composite materials.

DOI: 10.1103/PhysRevB.65.045322 PACS number(s): 78.47.+p, 73.40.−c, 07.79.Fc

I. INTRODUCTION

In many metal-semiconductor composite materials Schottky contacts are formed at the interfaces between the semiconductor and the metal inclusions. Around the Schottky contacts electric fields and potentials exist even if no external bias field is applied.[1] If charge carriers are optically excited in such a material, the dynamics of the carriers will be substantially influenced by the built-in electric fields. More specifically, the fields will separate positive and negative charges. This charge separation results in the generation of space charge, which, in turn, changes the electric field distribution. Thus, complex carrier and field dynamics can be anticipated. If the metal inclusions act as carrier trapping centers, one expects that the built-in fields also directly affect carrier trapping into the metal. This is because the electric fields lead to carrier transport towards or away from the metal-semiconductor interface, depending on the sign of the charge and the direction of the fields.

Without external bias, the electric field is nonzero only in the depletion zone of a Schottky contact with a typical extension in the micrometer or submicrometer range. This short length scale implies that the carrier dynamics occurs on a short time scale.[2] Therefore, only experimental techniques with both high temporal and high spatial resolution can provide detailed insight into the carrier dynamics close to a Schottky contact. As a consequence, femtosecond-resolved pump-probe measurements in the optical near-field (NF) lend themselves well to the study of carrier dynamics around Schottky contacts. This experimental technique has proven to be a powerful tool for the study of spatially resolved carrier dynamics in semiconductor nanostructures. Very recently, with this technique carrier drift and diffusion as well as relaxation dynamics have been explored in various structured semiconductors, such as patterned quantum wells[3] or quantum wires.[4,5]

In this paper, we present a comprehensive study of free carrier and field dynamics around nanoscale Schottky contacts. Experimental data are obtained using a recently developed femtosecond-resolved near-field scanning optical microscope (NSOM).[6,7] The experiments have been performed on a lithographically produced model system, which consists of tungsten (W) nanodisks embedded in GaAs. Earlier work has shown that Schottky contacts are formed around the W disks.[8] The lithographic fabrication process allows us to adjust the spacing between the disks so that the depletion zones of adjacent disks do not overlap.[8] In such samples, the femtosecond NSOM pump-probe measurements reveal the ultrafast carrier dynamics in the close vicinity of a *single* tungsten nanodisk in GaAs. Thus, we can directly observe the interplay between free carrier and field dynamics and carrier trapping around a *single* Schottky contact. This experimental approach avoids complications due to averaging over an ensemble of Schottky contacts, which arise in most far-field experiments. With respect to our choice of system, we would also like to mention that W-disk/GaAs structures have poten-

tial for semiconductor device technology as the electrical properties of the GaAs can be changed from conducting to semi-insulating by varying the disk spacing.[9]

Recently, we have reported on initial spatially and temporally resolved measurements of carrier dynamics around nanoscale W disks.[10] We have identified the metallic inclusions as efficient trapping centers at high optically excited carrier densities. The purpose of this paper is to present systematic experimental and theoretical investigations of the complex spatiotemporal carrier dynamics around nanoscale Schottky contacts in different carrier density regimes. We will introduce a theoretical model based on a self-consistent treatment of the drift-diffusion equation for the carriers and Poisson's equation for the electric field. The model allows us to calculate the electron and hole dynamics as well as the temporal and spatial variation of the electric field and potential around a single Schottky contact. Two different carrier density regimes are revealed by the measurements and the calculations. At lower carrier densities, the built-in electric field is only weakly reduced, leading to a repulsion of electrons from the Schottky barrier. Therefore electron trapping into the W disk is strongly suppressed. In contrast, at higher carrier densities, the built-in field is screened, resulting in an efficient diffusive electron transport towards and trapping into the W disk. In both density regimes, the experimental data and the numerical calculations are in very good agreement.

Another important metal-semiconductor composite material is annealed low-temperature (LT) grown GaAs, which can be produced without lithographic processing. Annealed LT-GaAs contains metallic As precipitates,[11] which can form Schottky contacts with the embedding GaAs.[11,12] Ultrafast carrier trapping times into the As precipitates[13] and high resistivity[14,15] make this metal-semiconductor composite material very attractive for many optoelectronic and photonic devices. Examples include terahertz emitters,[16] ultrafast photoconductive switches,[17] ultrafast all-optical switches,[18] and semiconductor saturable absorbers.[19] We will show in the last section of this paper that optical far-field experiments on annealed LT-GaAs can be described by the picture of carrier and field dynamics that has been deduced from the experiments on the W-disk material with Schottky contacts. The study of a *single* As precipitate in the NF is not possible as the typical distance between precipitates is well below 100 nm,[20] i.e., smaller than the spatial resolution of our ultrafast NSOM.

II. EXPERIMENT

In the following, first the tungsten disk sample is described. We explain the design and the fabrication of the sample as well as the process used to prepare the sample for near-field experiments. Subsequently, the annealed low temperature grown GaAs sample is described. The last part of Sec. II deals with the details of the ultrafast NSOM experiment.

A. W disk structure

The investigated tungsten disk sample has been grown by metalorganic vapor phase epitaxy (MOVPE). On a GaAs substrate we have grown AlAs/GaAs etch stop layers, a 20 nm GaInP protection layer and a 20 nm thick GaAs layer. Afterwards, W disks with ~80 nm diameter and a thickness of 20 nm have been deposited in a rectangular pattern with 2 μm disk spacing by electron beam lithography and a subsequent lift-off process. The disks have then been epitaxially overgrown with an 80 nm thick GaAs layer, followed by a 500 nm thick GaInP layer. The GaAs is *n*-doped (electron density $\sim 10^{16}$ cm^{-3}) and Schottky barriers are formed at the W/GaAs interface.[8,9] A detailed description of the fabrication process can be found in Refs. 8 and 9.

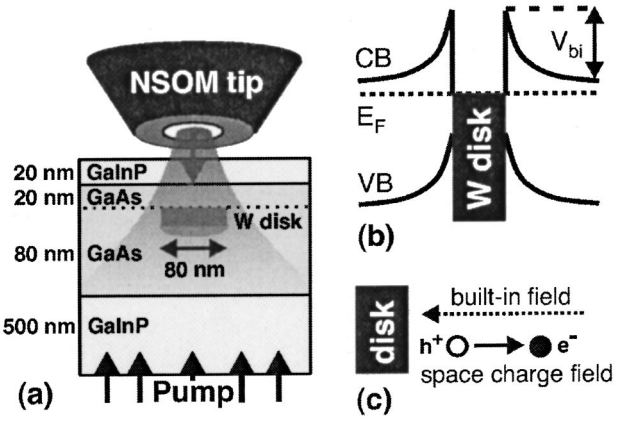

FIG. 1. (a) Schematic illustration of the tungsten disk sample, showing the GaAs layer with the embedded W disk, sandwiched between GaInP layers. Additionally, the global pump/local probe NSOM configuration is depicted. (b) Schematic diagram of the GaAs band structure with the bent conduction and valence band (CB and VB, respectively) and the Fermi energy (E_F) around the W disk. V_{bi} denotes the built-in potential. (c) Schematic illustration of the built-in electric field pointing towards the disk. The field separates electrons and holes. The resulting space-charge field points in the opposite direction as the built-in field.

Suitable samples for transmission NF measurements have to fulfill two main requirements. Light of the wavelength of interest should only be absorbed in the active region and the active region has to be as close as possible to the surface to preserve spatial resolution. Therefore we have glued our sample upside down on a glass substrate and removed the GaAs substrate and the etch-stop layers by chemical wet etching.[2] The remaining structure, schematically shown in Fig. 1(a), consists of the absorbing GaAs with the embedded W disks, sandwiched between GaInP layers, the bottom one as mechanical support and the top one as protection layer to avoid surface trapping of the optically excited carriers.

B. LT-GaAs sample

For comparison with the W disk sample we have designed an LT-GaAs sample, which is sufficiently *n* doped to expect large built-in fields close to the As precipitates. Additionally, we have grown an undoped LT-GaAs sample to measure the carrier dynamics in the presence of only weak built-in fields. The two 500 nm thick LT-GaAs samples have been grown on a GaAs substrate by molecular beam epitaxy (MBE) at As_4/Ga-flux ratios of 3 and 4.5, respectively, and a growth

temperature of 320 °C. One sample is undoped, the other one is *n* doped with Si at a concentration of 1×10^{18} cm^{-3}. This Si concentration has been chosen much larger than the concentration of ionized arsenic antisites As^{+}_{Ga}, which is smaller than 1×10^{17} cm^{-3}.[13,21] Therefore the majority of the doping electrons will contribute to the formation of Schottky contacts with large built-in fields. After the growth, both samples have been annealed *in situ* under arsenic overpressure at 600 °C for 1 h. Such conditions ensure the formation of metallic As precipitates.[11] For transmission measurements, the GaAs substrate has been removed by chemical wet etching.

C. Experimental setup

On the W-disk sample, we have performed degenerate NF pump-probe measurements at room temperature with 100 fs pulses, centered at a photon energy of 1.46 eV, from a 100 MHz mode-locked Ti:sapphire laser. A global pump/local transmitted probe configuration is used, as schematically depicted in Fig. 1(a). The W-disk sample is excited uniformly from the bottom side with a pump beam of ~10 μm diameter. The induced transmission changes are detected from the top side with a probe pulse, which propagates through a tube-etched, metal-coated NF fiber tip and the sample. To ensure high temporal resolution, the probe pulses are precompensated with a prism pair setup in front of the fiber. In Ref. 7 we have shown that with the described femtosecond NSOM we obtain a spatial resolution of 150 nm and a temporal resolution of 250 fs. In the same reference, one can find a more detailed description of the femtosecond NSOM. The far-field measurements on the LT-GaAs samples have been performed with the same setup in which the NSOM fiber has been replaced by a cleaved fiber, resulting in a probe spot diameter of ~4 μm on the sample. This data has also been taken at room temperature.

III. THEORETICAL MODEL

We have performed numerical simulations in order to obtain a better understanding of the experimental NF pump-probe data. The electron and hole density and the electric field in the vicinity of a W disk are calculated with the drift-diffusion equation and Poisson's equation in a self-consistent way. In our model, we neglect dynamics in the direction perpendicular to the W-disk plane. This simplification is justified by the geometry of the sample. The carriers are confined in a thin slab of 100 nm thick GaAs by the top and bottom GaInP layer. Therefore, carrier transport occurs mainly in the much larger W-disk plane. The symmetry of the W-disk structure then allows us to use a one-dimensional model with the radius r in the W-disk plane as the only space coordinate. The zero point is chosen at the center of the disk. The calculations of the electron/hole dynamics have been performed in an area extending from the W/GaAs interface at $r_{\mathrm{disk}}=40$ nm (r_{disk} radius of a single W disk) to $r=1$ μm. At $r=1$ μm the influence of the W disk on the carrier dynamics has found to be negligible.

The internal static electric field $E_{\mathrm{intern}}(r)$ inside the depletion region is obtained by a simple integration of Poisson's equation without optical excited carriers, analogous to the calculations in Ref. 1:

$$E_{\mathrm{intern}}(r)=\frac{qN_d}{2\varepsilon}\left(r-\frac{w^2}{r}\right).$$

Here, q is the electron charge, $N_d=10^{16}$ cm^{-3} the donor impurity density and ε the dielectric constant of GaAs. Outside the depletion region E_{intern} is zero. The position of the edge of the depletion zone is denoted by w, measured from the center of the W disk. This position w can be obtained from

$$V_{bi}=\frac{q^2N_d}{2\varepsilon}\left(w^2\ln\frac{w}{r_{\mathrm{disk}}}-\frac{1}{2}(w^2-r_{\mathrm{disk}}^2)\right).$$

Here, V_{bi} denotes the built-in potential. V_{bi} is given by the difference between the barrier height of the metal-semiconductor contact and the potential difference between the Fermi level and the conduction band energy outside the depletion region, see Fig. 1(b).

The dynamics of the electron density $n(r,t)$ depends on the total electric field E and the hole density $p(r,t)$ and is given by the continuity equation

$$\partial_t n(r,t)=D_n\left(\partial_r^2 n+\frac{1}{r}\partial_r n\right)+\mu_n\left(\frac{n}{r}\partial_r(rE)+E\partial_r n\right)-Bnp+g(t), \tag{1}$$

$$\partial_t n(r_{\mathrm{disk}},t)=-\frac{n(r_{\mathrm{disk}},t)}{\tau_n}. \tag{2}$$

The electron diffusion constant D_n and the mobility μ_n are linked by the Einstein relation and amount to 220 cm^2/s and 8500 cm^2/V s,[1] respectively. The term $-Bnp$ on the right-hand side of Eq. (1) accounts for bimolecular recombination. The spatially uniform carrier excitation is described by the r-independent generation term $g(t)$, for which we assume a sech^2 pulse with a full width at half maximum of 200 fs. The second equation describes the trapping of electrons into the disk at the W/GaAs interface, where τ_n denotes the trapping time. We have calculated τ_n multiplying the Richardson constant of 0.4 A cm^{-2} K^{-2} for electrons[22] with the surface of the W-disk shell of 5×10^{-11} cm^2 and the square of the room temperature. Following this procedure and dividing by the electron charge, a trapping time $\tau_n=90$ fs is deduced. This approach is based on the assumption that electron emission and trapping at the W/GaAs interface occurs at the same rate. Equivalent equations to Eqs. (1) and (2) are used to calculate the hole density $p(r,t)$. The corresponding values for D_p and μ_p are 10 cm^2/s and 400 cm^2/V s,[1] respectively. The trapping time $\tau_p=5$ fs is again obtained from the Richardson constant of 7 A cm^{-2} K^{-2} for holes.[22]

The electric field E is composed of the internal static field $E_{\mathrm{intern}}(r)$ and the space-charge field, which is related to the dynamics of the electrons and holes by the equations

$$E(r,t)=E_{\text{intern}}(r)+\frac{q}{\varepsilon r}\int_{r_{\text{disk}}}^{r} r'[Q_{\text{capt}}\delta(r'-r_{\text{disk}}) + p-n]dr', \tag{3}$$

$$Q_{\text{capt}}(t)=\int_{-\infty}^{t}\frac{p(r_{\text{disk}},t')}{\tau_p}-\frac{n(r_{\text{disk}},t')}{\tau_n}dt'. \tag{4}$$

The captured charge density Q_{capt} accounts for the trapped electrons and holes at the W/GaAs interface. The consideration of carrier trapping into the W disks in our model results in a time-dependent total electric field at $r=r_{\text{disk}}$ in contrast to previous works,[23,24] where trapping has been neglected. From the electric field we can deduce the electric potential $U(r,t)$ integrating the equation $E(r,t)=-\partial_r U(r,t)$. The integration has been performed for the boundary condition $U(r_{\text{disk}},t)=\text{const}$, i.e., the potential at $r=r_{\text{disk}}$ is kept fixed while it varies with time for $r>r_{\text{disk}}$. This choice of boundary condition emphasizes that the Schottky barrier height remains constant, whereas the potential barrier is changing. Note that, for the interpretation of the physics, only the potential difference between $r=r_{\text{disk}}$ and $r>r_{\text{disk}}$ matters.

All parameters for the calculations are taken from literature, except for the built-in potential V_{bi} and the bimolecular recombination constant B. Those parameters are obtained by comparing the simulations with the experimental results. We find for the built-in potential $V_{bi}=0.15$ eV, leading to the depletion region edge at $w=160$ nm. We like to recall that V_{bi} denotes the built-in potential and not the full Schottky barrier height. As shown in Fig. 1(b), V_{bi} is smaller than the full Schottky barrier height. The bimolecular recombination process is introduced, because the experiments have shown that the decay of the electron density far away from the disks is strongly dependent on the density. Such a behavior cannot be modeled by a monomolecular recombination process. From the comparison with the measurements, we deduce a bimolecular recombination constant of $B=5.6\times10^{-7}$ cm^3/s. The large value of B compared to the bimolecular *radiative* recombination constant [$\sim10^{-10}$ cm^3/s in GaAs (Ref. 25)] suggests that the bimolecular recombination process is nonradiative and possibly related to impurities.

The comparison of the experimental results with the numerical simulations and the discussion in Sec. IV are based on the assumption that the pump-probe traces directly reflect the carrier density dynamics in the GaAs.[26] As we detect the pump-induced transmission changes at an energy close to the band edge, the electrons yield the major contribution to the pump-probe signal.[27] Therefore, we compare the calculated electron density n to the experimental pump-probe data. In such comparisons, we convolute the calculated electron density n with a Gaussian function that accounts for the spatial resolution of 230 nm in the experiment.[28] If no comparison is made to experimental data, the calculated data are not convoluted, i.e., unlimited spatial resolution is assumed when presenting purely theoretical results. In this way, maximum information is obtained.

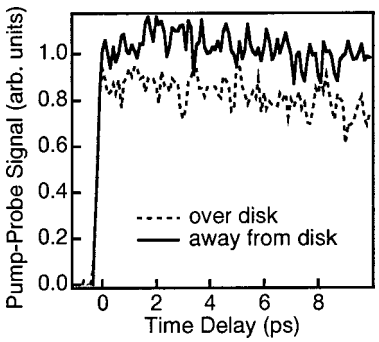

FIG. 2. Low-density regime: near-field pump-probe traces taken either over (dashed line) or 1 μm away (solid line) from the W disk.

IV. EXPERIMENTAL RESULTS AND DISCUSSION

In this section we will first present and discuss measurements and simulations of the carrier dynamics in the W-disk sample. Two different cases are considered, namely, carrier dynamics at lower and at higher optically excited carrier densities. With respect to our analysis of the carrier dynamics, we like to recall the properties of the built-in potential and field close to a Schottky contact before optical excitation. A schematic illustration is shown in Figs. 1(b) and 1(c), respectively. In the last part of this section, the W-disk results will be used to explain the data obtained in undoped and *n*-doped LT-GaAs.

A. Low-density regime

In this subsection, we will discuss the carrier and field dynamics for a low optically excited carrier density of 6×10^{15} cm^{-3}. Figure 2 shows pump-probe traces taken either over or 1 μm away from a W disk. Apart from a small difference in amplitude both traces look the same. The curves are essentially constant within the 10 ps time window of the measurement. No fast dynamics is observable, neither over the disk nor far away, in this experiment with a temporal resolution of 250 fs. We conclude that carrier trapping is inefficient despite the presence of a trapping center in form of the W disk.

Figure 3(a) shows a two-dimensional (2D) image of the pump-probe signal taken at a time delay of $\Delta t=2$ ps. In the center of the image, where the W disk is located, a clear reduction of the signal is visible. Around this region, one observes a ring-shaped region in which the nonlinear signal is slightly larger. The same features are seen in the 2D image of the calculated electron density in Fig. 3(b). The 2D images suggest electron transfer from the border of the disk to the outside region, leading to a reduction of the electron density over the disk and to an enhancement of the density at a distance of 200 nm around the disk. One might wonder why this process does not lead to a fast decaying contribution to the pump-probe trace in Fig. 2 that has been taken over the disk. The absence of such a fast decaying signal (Fig. 2) is due to the finite temporal resolution of $\sim$250 fs. We conclude that the electrons are redistributed already during the pump excitation pulse, resulting in the electron distribution seen in

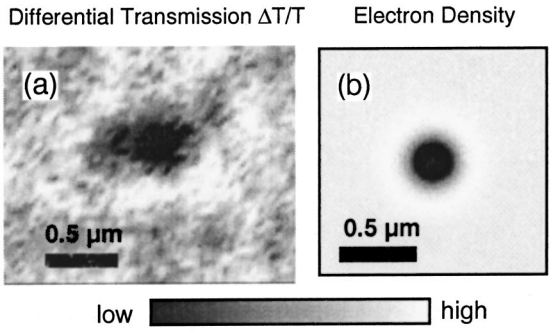

FIG. 3. Low-density regime: (a) two-dimensional optical near-field image of the differential transmission $\Delta T/T$ taken at a time delay $\Delta t = 2$ ps over a single W disk at an optically excited carrier density of 6×10^{15} cm^{-3}. (b) Calculated electron density obtained from the theoretical model of Sec. III for the experimental conditions of (a).

Fig. 3 at $\Delta t = 2$ ps. This interpretation is confirmed by the numerical simulations that will be discussed next. The numerical simulations also confirm that carrier trapping into the W disk is inefficient in the low-density regime and elucidate the reason for this experimental finding.

With regard to the simulations, we would like to emphasize that very good agreement between the calculated and the experimental data is obtained in Fig. 3. This result testifies to the validity of the model presented in Sec. III. In particular, it is a valid procedure to identify the pump-probe signal with the electron density and to neglect hole contributions, many-body effects,[26] and field-induced transmission changes due to the Franz-Keldysh effect.[29] As a consequence, we can extract the spatial dependence and the temporal evolution of important parameters from the model.

Figure 4 shows the electron density n, the hole density p, the total electric field E, and the (energy) potential $-|q|U$ vs distance r from the center of the disk for different time delays Δt. We begin with the discussion of the total electric field E and the potential $-|q|U$. Later, we will comment on the dynamics of the electrons and holes. We would like to recall that all four variables n, p, E, and $-|q|U$ are coupled by the equations of Sec. III and, therefore, should always be considered together.

In Fig. 4(a) we show the temporal evolution of the total electric field. The trace at time delay $\Delta t = -1$ ps indicates the built-in field before optical excitation. The field is negative as it points towards the disk. After optical excitation the electron-hole pairs are separated by the electric field. The holes drift towards the disk, where they get trapped at the W/GaAs interface whereas the electrons drift away from the disk. The spatially separated electrons and holes induce a space charge field that is opposite to the built-in field; see the schematic picture of Fig. 1(c). Therefore, we find that the absolute value of the electric field decreases to less than half of its initial value within the first 10 ps. This behavior is reflected by the evolution of the energy potential in Fig. 4(b). The potential barrier is reduced to a third of its initial value within the first 10 ps. The field and the energy potential remain almost unchanged for several tens of picoseconds (data not shown). For example, the curves at $\Delta t = 10$ ps and

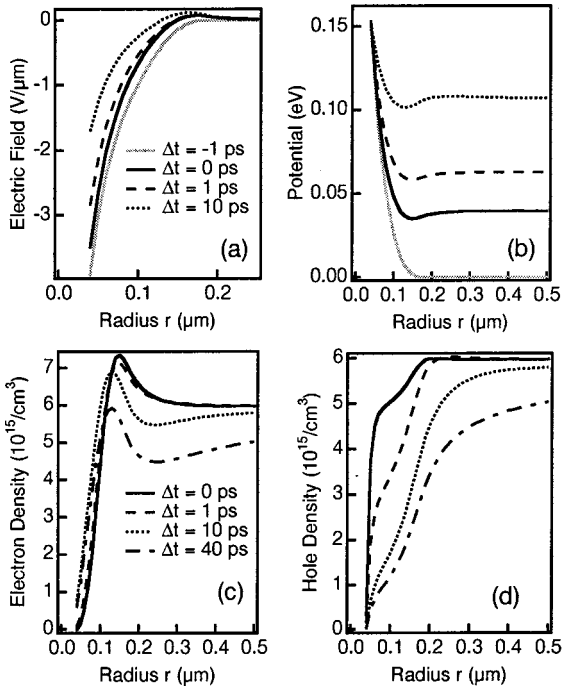

FIG. 4. Low-density regime: results form the theoretical model plotted vs radius r from the center of the W disk at different time delays Δt. (a) Electric field, (b) energy potential, (c) electron density, and (d) hole density. In (a) and (b) the traces at $\Delta t = -1$ ps indicate the electric field and the potential before optical excitation. The legend in (a) also applies to (b). Likewise, the legend in (c) applies to (d). Note the different r scale in (a).

$\Delta t = 40$ ps almost coincide. We like to emphasize that a considerable field and potential barrier remain after optical excitation. The remaining electric field leads to a non-negligible electron drift current away from the disk, which counteracts electron diffusion towards the disk. Thus, net electron transport to the disk is reduced and the trapping of electrons into the disk is inefficient, as seen from the pump-probe traces of Fig. 2.

Focusing now on details of the field dynamics, one observes a sign change of the electric field and a dip in the potential at $r = 0.14$ μm already at very early time delays ($\Delta t = 0$ ps). The positive electric field for $r > 0.14$ μm reflects the increase of the potential that leads to the formation of a potential well. The well is self-induced by the electron and hole dynamics and the resulting space-charge field, i.e., it arises from the coupling of the carrier and the electric field dynamics. From the discussion in the previous paragraph, it follows that the well persists up to 40 ps.

The temporal evolution of the electric field and the potential are closely related to the electron and hole dynamics shown in Figs. 4(c) and 4(d), respectively. Already during the pump excitation ($\Delta t = 0$ ps) the electrons are efficiently pulled away from the W disk by the electric field and accumulate at the edge of the depletion zone. This numerical result is in agreement with the absence of a fast contribution in the pump-probe traces of Fig. 2. The maximum in the electron density seen in Fig. 4(c) is consistent with the dip in the potential and the sign change of the electric field. In other

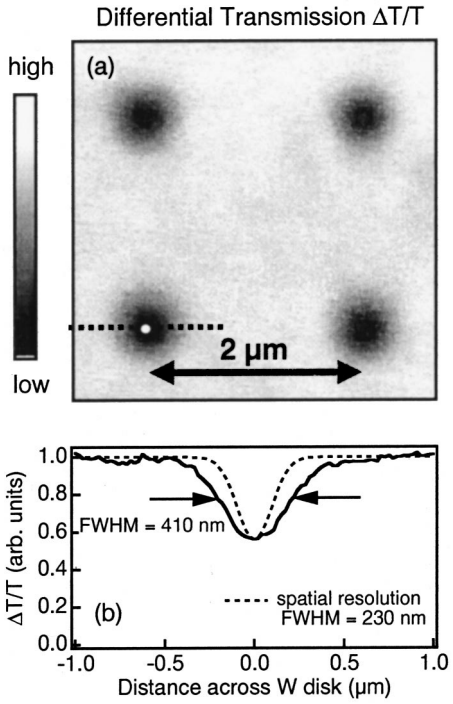

FIG. 5. High-density regime: (a) two-dimensional image of the differential transmission $\Delta T/T$ at time delay $\Delta t = 15$ ps. The white disk in the lower left corner schematically marks the size of a W disk. (b) Line scan of the differential transmission $\Delta T/T$ (solid line) along the dashed line in (a) together with the Gaussian function showing the spatial resolution (dashed line). FWHM: full width at half maximum.

words, the electrons accumulate in the potential well. The maximum in the electron density is the reason for the ring-shaped signal enhancement in Fig. 3. The maximum is still seen at $\Delta t = 40$ ps, corresponding to the long lifetime of the potential well.

The hole dynamics in Fig. 4(d) is dominated by hole drift and diffusion towards and trapping into the disk. These processes are slower than the corresponding electron processes due to the smaller hole mobility and diffusion constant. Nevertheless, these processes substantially reshape the hole distribution during the first 40 ps. In particular, diffusion smoothes the hole distribution. The weak overall reduction of both the electron and hole density is due to the inefficiency of bimolecular recombination at low carrier density.

B. High-density regime

In the high-density regime we consider an excited carrier density of $7-8\times10^{16}$ cm^{-3}, which is significantly higher than the doping level. Figure 5(a) shows a 2D image of the pump-probe amplitude at a time delay of 15 ps. The disk pattern is clearly visible as the measured signal is substantially reduced over the disks. In Fig. 5(b) we show a line scan of the pump-probe signal together with a Gaussian function that indicates the spatial resolution in the experiment. The electron density is reduced not only over the disks, but also in a wide region around the disks. This region has a full width at half maximum (FWHM) of 410 nm and is much broader than the spatial resolution function with a FWHM of 230 nm. We conclude that the electrons from this region have moved towards the disk, where they have been trapped, in contrast to the dynamics seen in the low-density regime. Efficient electron transport towards the disks is only possible if the built-in field is screened.[10] Otherwise electron drift away from the disks counteracts diffusion towards them, suppressing net electron transport. This reasoning indicates that diffusion is the main transport mechanism for electrons under this experimental condition.

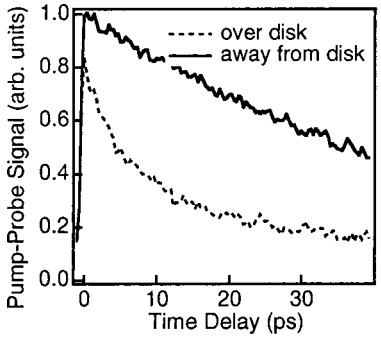

FIG. 6. High-density regime: near-field pump-probe traces taken either over (dashed line) or 1 μm away (solid line) from the disk.

In Fig. 6, pump-probe traces are shown, which have been taken either over or 1 μm away from the disk. Over the disk, the signal decays within 7.5 ps to half of its initial value, significantly faster than away from the disk, where it takes 37 ps to reach the half-maximum point. Both traces decay faster than the corresponding low-density curves in Fig. 2. This data confirms that efficient electron trapping takes place in the high-density regime. Note that the density dependence of the bimolecular recombination cannot be the main reason for the results in Fig. 6. This is because bimolecular recombination alone would not lead to different decays at different positions.

More details of the spatiotemporal carrier dynamics can be inferred from direct measurements of the pump-probe signal versus distance across a single W disk for fixed time delays Δt. These data together with the simulated electron density are shown in Fig. 7(a). At zero time delay, the electron density is mainly reduced in the close vicinity of the W disk. With time, the shape of the traces changes and a reduction of the electron density is also observed farther away from the disk. The calculated electron density agrees very well with the measured pump-probe line scans. The good agreement shows that the model of Sec. III is also valid in the high-density regime. We will later on deduce details of the carrier and field dynamics from the model.

Figure 7(b) shows how the FWHM of the dip increases with time. After an initial fast broadening of the signal dip, the increase of the FWHM slows down at longer time delays. A fast broadening of the carrier density dip has been found in quantum wells with artificially introduced trapping centers.[3] In such samples, only trapping and diffusion determine the carrier dynamics; carrier drift does not contribute. Therefore, the data of Fig. 7 suggest that the electron dynamics is strongly affected by diffusion during the first several picoseconds when the broadening of the pump-probe dip is pro-

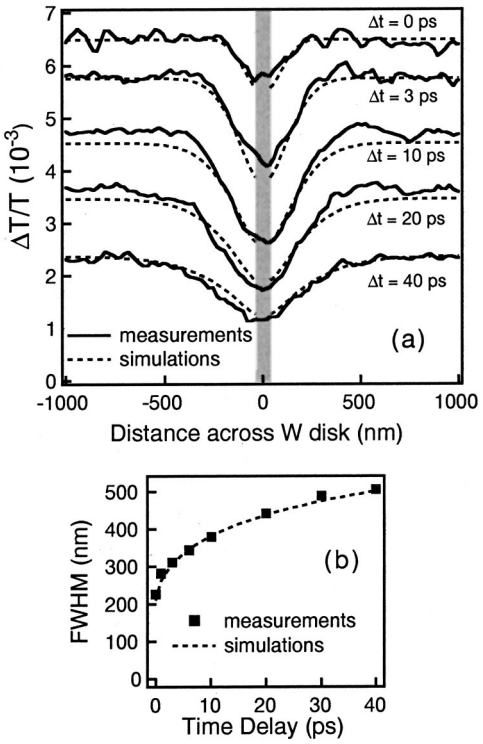

FIG. 7. High-density regime: (a) Line scans of the measured differential transmission signal (solid lines) and the calculated electron density (dashed lines) across a single tungsten disk for different time delays Δt. The gray bar marks the extension of the tungsten disk. (b) Full width at half maximum (FWHM) of Gaussian fits to the measured curves (squares) and FWHM of Gaussian fits to calculated traces (dashed line).

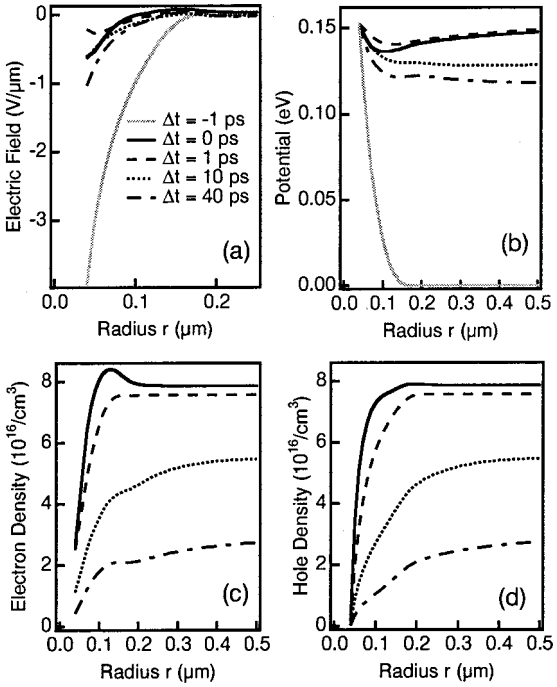

FIG. 8. High-density regime: Results form the theoretical model in the high-density regime plotted vs radius r from the center of the W disk at different time delays Δt. (a) Electric field, (b) energy potential, (c) electron density, and (d) hole density. In (a) and (b) the traces at $\Delta t = -1$ ps indicate the electric field and the potential before optical excitation. Traces for $\Delta t = -1$ ps are not shown in (c) and (d). The legend in (a) also applies to (b)–(d). Note the different scale in (a).

nounced. The overall signal reduction is due to the bimolecular recombination, which is efficient at high carrier densities.

Summarizing the results of Figs. 5–7, the experimental data indicate that the electric field is strongly screened in the high-density regime, giving rise to efficient diffusive transport of electrons towards the W disk and efficient electron trapping. These results are reconfirmed by the numerical simulation shown in Fig. 8. Figure 8(a) demonstrates that the electric field is considerably suppressed almost immediately after excitation, in contrast to the low-density regime. Likewise, the energy potential is almost flat, as shown in Fig. 8(b). In the high-density regime, where the excitation density is well above the doping level, already at short times the built-in field is efficiently screened by the large amount of holes that are rapidly trapped into the W disk. At longer time delays the electric field and the potential slowly recover. The recovery is clearly seen if one compares the potential curves at 1 and 40 ps in Fig. 8(b).

In Figs. 8(c) and 8(d) we present the calculated electron and hole densities. During the excitation at $\Delta t = 0$ ps the electrons are removed from the W-disk border by the internal electric field and we observe a maximum of the electron density at the edge of the depletion zone [Fig. 8(c)]. Compared to the low-density situation this drift induced process is weaker at higher densities and disappears almost immediately.[30] Following the optical excitation, the electric field rapidly breaks down. As a consequence, drift contributions can be neglected and diffusion dominates the carrier transport in the first 10 ps after excitation. Electrons and holes are transferred to the disk, where they get trapped and recombine. The diffusion dynamics is driven by the carrier density gradient resulting from carrier trapping into the W disk. Additionally, diffusion smoothes out the electron and hole density profiles and therefore leads to the broadening of the pump-probe signal dip seen in Fig. 7(b).

As the diffusion is faster for electrons than for holes, the charge of the initially trapped holes is slowly compensated. This process and the significant reduction of the carrier density due to efficient carrier trapping and bimolecular recombination result in the slow recovery of the built-in electric field and the potential. Once the potential barrier has acquired a sufficient height, it again suppresses electron transport towards the disk. Therefore, electron trapping becomes less efficient at longer times. The suppression of electron transport and trapping at longer times is observed in Fig. 6. Figure 6 shows that the decrease of the pump-probe signal over the disk significantly slows down for long time delays, resulting in a signal offset.

C. Annealed LT-GaAs

The results obtained from the study of the W-disk model sample for nanoscale Schottky contacts can now be used to discuss the carrier dynamics in annealed LT-GaAs. Figure 9

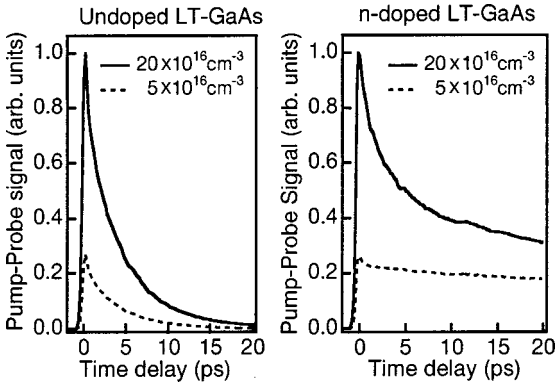

FIG. 9. Far-field pump-probe traces of undoped (a) and *n*-doped (b) annealed LT-GaAs samples taken at low (dashed lines) and high (solid lines) excitation carrier densities.

shows pump-probe signals for low and high optically excited carrier densities in undoped and *n*-doped LT-GaAs. The excitation photon energy is 1.46 eV. As shown in Fig. 9(a), in the undoped sample the signal decays exponentially for both low and high carrier densities with a typical $1/e$ time of 3.5 ps. We find the same decay even for carrier densities below 10^{15} cm^{-3} (data not shown). In Ref. 13 it has been shown that the decay of the pump-probe signal in undoped LT-GaAs is due to electron trapping into As precipitates. Figure 9(a) shows that the efficiency of this fast trapping process is independent of the optically excited carrier density. We recall that electrons have first to move to the precipitates before being trapped at the metal/semiconductor interface. Therefore, we conclude that the built-in fields of the Schottky contacts around the precipitates in the undoped annealed LT-GaAs sample are too small to substantially suppress electron transport towards the As precipitates even at very low densities.

In contrast, the pump-probe signals in the *n*-doped sample show a strong carrier density dependence, as seen in Fig. 9(b). At high carrier densities, we find a fast initial decay that slows down at later times, resulting in an offset. At low carrier densities, there is no significant fast reduction of the signal, but the signal remains almost constant over the whole time window of the measurement. This behavior is very similar to the carrier dynamics that have been observed in the W-disk sample at low (Fig. 2) and high (Fig. 6) carrier densities. Therefore we conclude that the underlying physics is the same in both cases. As expected from the design of the *n*-doped LT-GaAs sample, our data indicate that strong built-in electric fields are present around the Schottky contacts before optical excitation in the *n*-doped LT-GaAs. At low optically excited carrier densities the fields suppress electron transport towards and trapping into the As precipitates. In contrast, at high carrier densities above the *n*-doping level, the trapped holes substantially screen the built-in fields, resulting in efficient diffusion and trapping of electrons. The electron transport is again suppressed when the optically excited electron density has substantially decreased to a value comparable to the doping level.

V. CONCLUSION

We have presented a detailed study of the carrier and field dynamics around Schottky nanocontacts for different optically excited carrier densities. Tungsten disks embedded in GaAs have been investigated by femtosecond near-field optics. The dynamics has been modeled by the drift diffusion and Poisson's equation. Experiments and numerical simulations agree very well and reveal two different density regimes. The low-density regime is characterized by the transfer of electrons away from the disk and their accumulation at the edge of the depletion zone. As the holes move towards the disk, a space-charge field is formed which points in the opposite direction as the built-in field. However, the space-charge field is weak. The total field and the corresponding potential barrier are still strong enough to suppress electron transport towards and electron trapping into the W disk. Hence, the optically excited electrons live for a long time outside the depletion region.

In the high-density regime, the built-in field is substantially screened by the trapped holes leading to efficient electron transport towards and trapping into the W disk. Once the carrier density is considerably reduced, the built-in electric field is restored and electron trapping is again suppressed. These results demonstrate that the coupling of the carrier and field dynamics can substantially affect carrier trapping in metal-semiconductor composite materials in which Schottky contacts are formed.

As a second metal-semiconductor composite material, we have investigated annealed LT-GaAs, in which Schottky contacts are formed around metallic As precipitates. We have shown that the carrier dynamics significantly depends on the doping density of the LT-GaAs. In *n*-doped LT-GaAs, the dynamics is very sensitive to the optically excited carrier density: a fast decay of the electron population is observed at high densities and a slow one at low densities. In contrast, in undoped LT-GaAs, the electron population decays rapidly independent of the optically excited carrier density. Thus, the doping concentration and the optically excited carrier density are important parameters for the recovery time of devices produced from annealed LT-GaAs. We attribute the observed effects to the screening of the built-in fields and conclude that the same mechanisms are at work as in the W-disk sample.

ACKNOWLEDGMENTS

The authors wish to thank M. Haiml for many helpful discussions about LT-GaAs. Moreover, for some near-field measurements we obtained good NSOM tips from A. Bouhelier.

*Electronic address: acherman@iqe.phys.ethz.ch

[1] S. M. Sze, *Physics of Semiconductor Devices* (Wiley, New York, 1981).
[2] U. Siegner, M. Achermann, and U. Keller, Mat. Sci. Tech. **12**, 1847 (2001).
[3] M. Achermann, B. A. Nechay, F. Morier-Genoud, A. Schertel, U. Siegner, and U. Keller, Phys. Rev. B **60**, 2101 (1999).
[4] V. Emiliani, T. Guenther, C. Lienau, R. Nötzel, and K. H. Ploog, Phys. Rev. B **61**, R10 583 (2000).
[5] M. Achermann, B. A. Nechay, U. Siegner, A. Hartmann, D. Oberli, E. Kapon, and U. Keller, Appl. Phys. Lett. **76**, 2695 (2000).
[6] B. A. Nechay, U. Siegner, F. Morier-Genoud, A. Schertel, and U. Keller, Appl. Phys. Lett. **74**, 61 (1999).
[7] B. A. Nechay, U. Siegner, M. Achermann, H. Bielefeldt, and U. Keller, Rev. Sci. Instrum. **70**, 2758 (1999).
[8] L.-E. Wernersson, N. Carlsson, B. Gustafson, A. Litwin, and L. Samuelson, Appl. Phys. Lett. **71**, 2803 (1997).
[9] L.-E. Wernersson, A. Litwin, L. Samuelson, and W. Seifert, Jpn. J. Appl. Phys., Part 2 **36**, L1628 (1997).
[10] M. Achermann, U. Siegner, L. E. Wernersson, and U. Keller, Appl. Phys. Lett. **77**, 3370 (2000).
[11] A. C. Warren, J. M. Woodall, J. L. Freeouf, D. Grischkowsky, M. R. Melloch, and N. Otsuka, Appl. Phys. Lett. **57**, 1331 (1990).
[12] R. M. Feenstra, A. Vaterlaus, J. M. Woodal, and G. D. Pettit, Appl. Phys. Lett. **63**, 2528 (1993).
[13] M. Haiml, U. Siegner, F. Morier-Genoud, U. Keller, M. Luysberg, R. C. Lutz, P. Specht, and E. R. Weber, Appl. Phys. Lett. **74**, 3134 (1999).
[14] J. F. Whitaker, Mater. Sci. Eng., B **22**, 61 (1993).
[15] G. L. Witt, Mater. Sci. Eng., B **22**, 9 (1993).
[16] C. Ludwig, J. Kuhl, Appl. Phys. Lett. **69**, 1194 (1996).
[17] T. Motet, J. Nees, S. Williamson, and G. Mourou, Appl. Phys. Lett. **59**, 1455 (1991).
[18] H. S. Loka and P. W. E. Smith, IEEE Photonics Technol. Lett. **10**, 1733 (1998).
[19] U. Keller, K. J. Weingarten, F. X. Kärtner, D. Kopf, B. Braun, I. D. Jung, R. Fluck, C. Hönninger, N. Matuschek, and J. Aus der Au, IEEE J. Sel. Top. Quantum Electron. **2**, 435 (1996).
[20] E. S. Harmon, M. R. Melloch, J. M. Woodall, D. D. Nolte, N. Otsuka, and C. L. Chang, Appl. Phys. Lett. **63**, 2248 (1993).
[21] X. Liu, A. Prasad, W. M. Chen, A. Kurpiewski, A. Stoschek, Z. Liliental-Weber, and E. R. Weber, Appl. Phys. Lett. **65**, 3002 (1994).
[22] M. Missous and E. H. Rhoderick, J. Appl. Phys. **69**, 7142 (1991).
[23] T. Dekorsy, T. Pfeifer, W. Kütt, and H. Kunz, Phys. Rev. B **47**, 3842 (1993).
[24] R. Kersting, J. N. Heyman, G. Strasser, and K. Unterrainer, Phys. Rev. B **58**, 4553 (1998).
[25] B. E. A. Saleh and M. C. Teich, *Fundamentals of Photonics* (Wiley, New York, 1991).
[26] J. Shah, *Ultrafast Spectroscopy of Semiconductors and Semiconductor Nanostructures* (Springer-Verlag, Berlin, 1999).
[27] R. Tommasi, P. Langot, and F. Vallée, Appl. Phys. Lett. **66**, 1361 (1995).
[28] As the W disk plane is 40 nm away from the NSOM tip, the spatial resolution is reduced to 230 nm even though the aperture of the tip is smaller.
[29] H. Heesel, S. Hunsche, M. Mikkelsen, T. Dekorsy, K. Leo, and H. Kurz, Phys. Rev. B **47**, 16 000 (1993).
[30] The maximum of the electron density is not visible in Figs. 5 and 7, because it is very weak. Moreover it is averaged out due to limited spatial resolution.